Available online at www.sciencedirect.com
SCIENCE DIRECT®

Journal of the European Ceramic Society 24 (2004) 3235–3243

www.elsevier.com/locate/jeurceramsoc

Oxidation kinetics of LaB_6 in oxygen rich conditions

Chung-Han Wen, Tsung-Ming Wu, Wen-Cheng J. Wei*

Institute of Materials Science and Engineering, National Taiwan University, Taipei, Taiwan, 106, ROC

Received 4 August 2003; received in revised form 28 October 2003; accepted 2 November 2003

Abstract

This paper investigated the oxidation behavior of LaB_6 in the temperature range of 700–1185 °C. The results obtained by thermogravimetric analysis (TGA) showed that the initial oxidation has parabolic kinetics in the temperatures between 800–945 °C. The oxidation process exhibited temperature dependence with an activation energy of 195±15 kJ/mol in air and in pure oxygen atmosphere. Two possible reactions, either the evaporation of B_2O_3 species (occurring ⩾945 °C) or the oxidation of surface LaB_6 (⩽800 °C), influence the oxidation mechanism to be interfacial reaction control, which results in mass loss deviating from parabolic behavior. The details of the microstructure evolution of the formation of glass and crystalline $La(BO_2)_3$ grains are investigated. The effects of porosity, the melting of $La(BO_2)_3$, coarsening of $La(BO_2)_3$ grains are reported and discussed.

Keywords: B_2O_3; LaB_6; La $(BO_2)_3$; Oxidation; Kinetics

1. Introduction

LaB_6 is an electron-offering material, which has been extensively used as the material of electronic guns for thermal emission electron microscope. The covalent bonds between boron atoms cause high melting temperature, and can be useful for the application in the high temperature environment. Similar to the borides of the fourth, fifth, and sixth periodic groups, LaB_6 has metallic appearance and properties, which are evidenced by their high electrical conductivity, low working function, and positive temperature coefficient of electrical resistance.[1]

Previous literature has studied mainly on ZrB_2 or the other rare earth borides, but not on the LaB_6 material. Berkowitz-Mattuck[2] reported that the oxygen-consumed law of ZrB_2 between 927–1727 °C was only parabolic relation was observed. For the temperatures greater than 1127 °C, the activation energy of the oxidation of ZrB_2 is 321 kJ/mol. Below 1127 °C the activation energy is much lower about 105 kJ/mol. The summary of the test results is shown in Table 1. The mechanisms of the oxidation of ZrB_2 are different and may be influenced by the presence of oxidized product B_2O_3, which would vaporize at high temperature. When the temperature is lower than 1027 °C, the parabolic rate constant appears increasing with oxygen partial pressure.[3]

Similarly, Tripp and Graham[4] reported the oxidation test of ZrB_2 in the range of 800–1500 °C. When the temperature is below 1000 °C, the activation energy is about 105 kJ/mol, and activation energy is 196.5 kJ/mol when higher than 1000 °C. The oxidation results showed an increasing deviation from parabolic law with increasing temperature, which might also concern with the vaporization of B_2O_3. They reported when the temperature was greater than 1000 °C, B_2O_3 had an appreciable vapor pressure, since the B_2O_3 melted above 450 °C,[4] at which ZrO_2 was produced and mixed with the liquid B_2O_3.

The oxidation of TiB_2 was also investigated[5,6] The TiB_2 starts to oxidize from 400 °C, and the oxidation resulted in crystalline TiO_2 and amorphous B_2O_3 at about 1000 °C[7] under high oxygen partial pressure. Table 1 also shows the data of obtained from various borides, e.g. HfB_2 and LaB_6–ZrB_2 composite. It is noted that the activation energy of the LaB_6–ZrB_2 composite is determined to be 130 kJ/mol which is identical to that of LaB_6 at the temperature range of 912–1053 °C.[8]

* Corresponding author. At present address: 1 Roosevelt Rd. Sec. 4, Taipei, Taiwan 106, ROC.
E-mail address: wjwei@ntu.edu.tw (W.-C. J. Wei).

0955-2219/$ - see front matter © 2003 Elsevier Ltd. All rights reserved.
doi:10.1016/j.jeurceramsoc.2003.11.016

The objectives of this research are to confer the oxidation kinetic behavior of LaB_6 at high temperature, and report the temperature dependent behavior. We also investigate the oxidizing microstructure by SEM and TEM, to realize the effects of oxidation temperature, atmosphere, and porosity in bulky LaB_6.

2. Experimental procedure

LaB_6 samples are 99.5% in purity and have a sintered density of 3.61g/cm^3, which is correspondent to 13 vol.% open porosity. Sample surfaces were ground by No. 1000 mesh SiC sandpaper, and cleared in a supersonic bath for 15 min. Each pure LaB_6 sample blocks in about $1\times1\times0.5$ cm^3 dimensions were prepared and measured by precise micro-meter after cutting and polishing the surface. Fig. 1 shows the surface morphology of as-polished LaB_6 bulky sample. The pore size on the surface is about 1–3 μm.

The oxidation behavior of LaB_6 was studied by a thermogravimetric (TG) system (CHAN 2000, Japan) between 700–1185 °C with an air or pure oxygen in a flow rate of 100 mL/min. The TGA equipment was connected with a bottom-heated furnace, which would allow the sample sliding into testing hot zone of the furnace and getting equilibrium in 1 min. Therefore, the mass change could be detected precisely at every set temperature.

Table 1
Activation energy of various borides oxidized in specified condition

Material	Temp. range (°C)	Q, kJ/mol (kcal/mol)	Ref.
ZrB_2	1127–1727	321 (77±5)	Berkowitz (1966)[2]
	927–1127	105 (25±6)	
ZrB_2	1000–1500	196.5 (47)	Tripp et al. (1971)[4]
	800–1000	105 (25)	
HfB_2	1200–1560	196.5 (47)	Berkowitz (1966)[2]
LaB_6–ZrB_2	912–1053	130 (31)	Chen et al. (2001)[8]
LaB_6	912–1053	130(31)	Chen et al. (2001)[8]

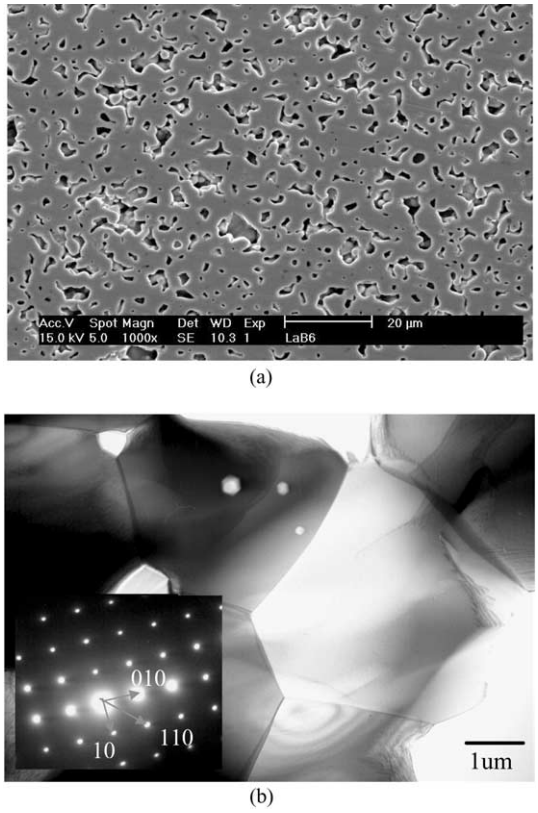

Fig. 1. (a) SEM and (b) TEM micrographs of polished LaB_6 without heat treatment, and the diffraction pattern of one LaB_6 grain.

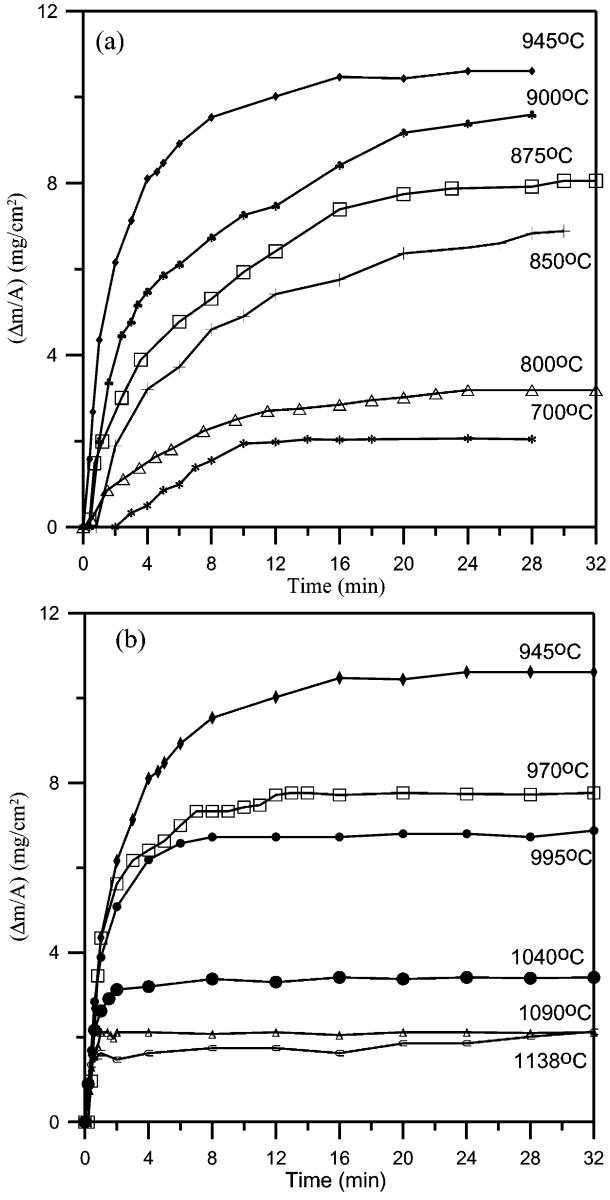

Fig. 2. Mass gain per unit area of bulky LaB_6 versus testing period in the temperature range of (a) 700–945 °C, and (b) 945–1138 °C. The samples were tested in air.

The samples were also examined by XRD (Philips PW1710, Philips Co., Netherlands) to evaluate the crystal phases resulted from the oxidation of LaB_6 undergone the thermal treatment in TGA. SEM(Philips XL30—SEM, Netherlands and Field Emission SEM, Leo Instrument 1530, England)—equipped with Energy Dispersive Spectrum (EDS) and was also used to observe the change of the microstructure of as-received and thermally treated samples. Amorphous phase was analyzed by the TEM (Jeol 100CXII, and Hitachi Model HF-2000 FEEM, Japan). In order to get representative thin foil samples for TEM observation, the thin foil samples were tested by TGA at 800 °C and 945 °C for 30 s to 8 min, then ion-milled again for 5 min. The oxide scale and partially oxidized grains were retained and could be observed by TEM.

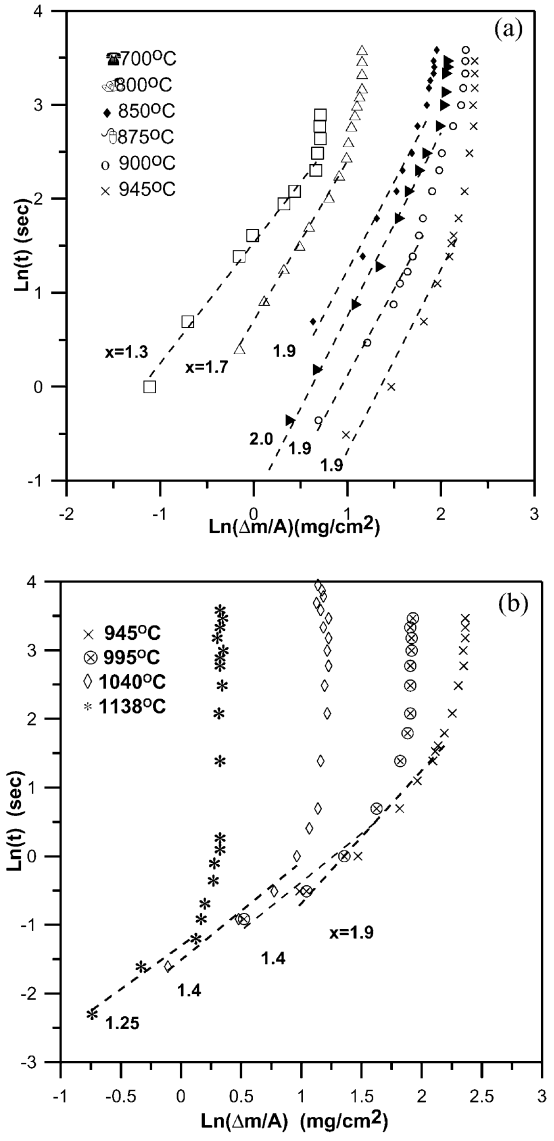

Fig. 3. Oxidation period as a function of specific mass change illustrating best fitted lines taken from the first few data points. The values of x are the slopes of the broken lines.

3. Results and discussion

3.1. Oxidation kinetics of LaB_6

The mass change of the samples tested in the temperatures ranging from 700 °C to 1188 °C is shown in Fig. 2. The mass change data were continuously collected for a period of time (less than 32 min) at each temperature. The mass change as a function of time in the range of temperatures 700–945 °C behaves different than that recorded at temperature higher than 945 °C. In the temperature range of 1040–1138 °C [Fig. 2(b)], the mass gain of every curve stops within 2 min. The same behaviour was also found for those sample tested at 970–1040 °C, but takes longer time to reach mass equilibrium. According to the data tested below 970 °C, the relationship between mass change (Δm) per unit time (t) and unit surface area (A) may obey the following rate equation.

$$(\Delta m/A)^x = k_p t. \quad (1)$$

The relation between $\ln(\Delta m/A)$ and ln(t) is shown in Fig. 3. Taking the best fitting of the slopes in the range of the first 7 data points in Fig. 2(a), the best fitting slopes in the graph give the values of x, which tells the oxidation dependence on time in this system. The value of x of every fitting slope is obtained and shown in Table 2. The oxidation behavior of the tests between 850–945 °C obeys the parabolic law when the value of x approximates to 2.0. So the main mechanism in the temperature region (850–945 °C) is diffusion control, which is limited by the diffusion of reactant through the oxidation products.

Fig. 3(a) and (b) depict that the values of x can be less than 2.0, and as small as 1.25. The result may indicate other reactions, e.g. surface-control or the evaporation of oxides, also affects the behavior of mass change. The oxidation of LaB_6 deviates from diffusion control at temperatures below 850 °C and greater than 945 °C.

Due to the values of x approximate to 2.0 below 945 °C, we obtain the relation of square specific mass change $(\Delta m/A)^2$ to the time (t), and shown in Fig. 4.

Table 2
Time exponent ($1/x$) of the oxidation tested at various temperatures

Temperature (°C)	X
700	1.3
800	1.7
850	1.9
875	2.0
900	1.9
945	1.9
995	1.4
1040	1.4
1138	1.25

The relationship shows that the oxidizing mass may deviate from linear dependence after holding at the temperature for a period of time. If taking the initial slope k_p fitted from first 7 data points, the scaling rate constant in Eq. (1) can be obtained at different temperatures. The value of k_p increases with raising temperature in the range of 800–945 °C on account of the faster oxidizing reaction rate. The value of activity energy of the oxidation can be calculated from the Eq. (2).

$$k_p = k_0 \times \exp(-Q/RT) \quad (2)$$

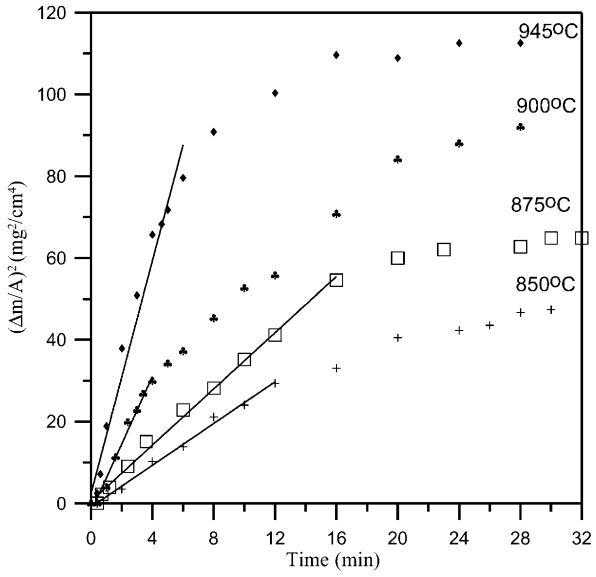

Fig. 4. Specific mass ($\Delta m/A$) changed as a function of oxidation period at temperatures 800–945 °C.

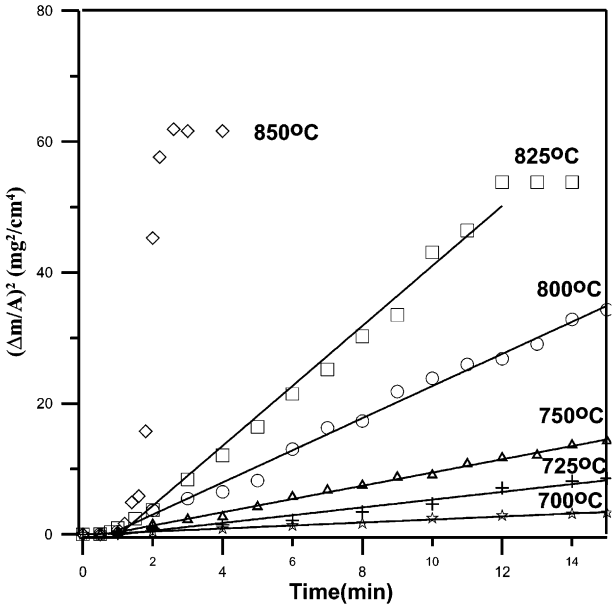

Fig. 5. Specific mass ($\Delta m/A$) changes as a function of oxidation period tested in pure oxygen at temperature range from 700–850 °C.

A comparison of the test was also conducted in high-purity oxygen (99.99%) atmosphere by TGA, but conducted at the temperatures ranging from 700 °C to 850 °C. The mass changes as a function of testing time are shown in Fig. 5.

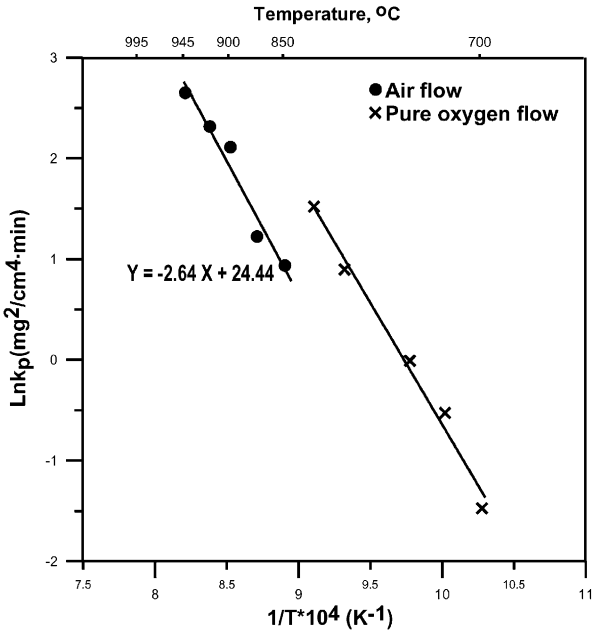

Fig. 6. Arrhenius plot of oxidation test of pure LaB_6 indicating an activation energy $Q = 195 \pm 15$ kJ/mol in air and $Q = 200 \pm 10$ kJ/mol in pure oxygen.

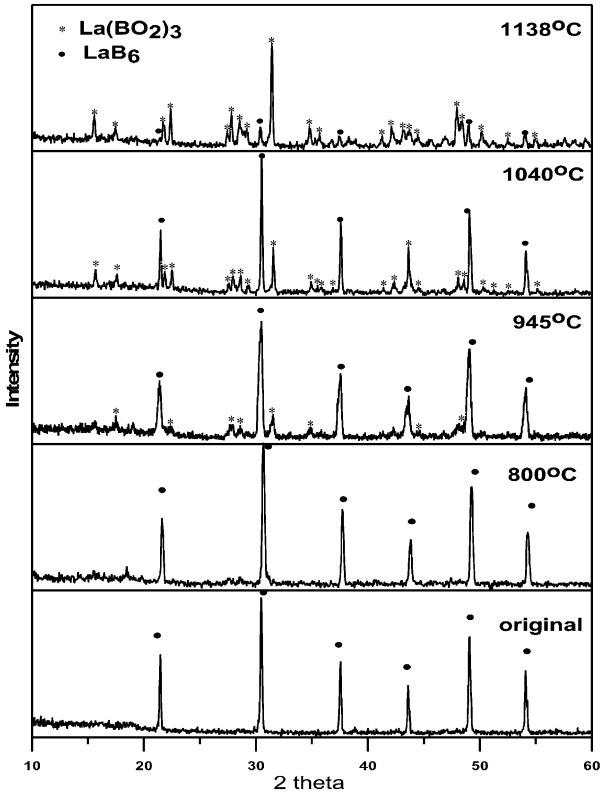

Fig. 7. XRD patterns of LaB_6 oxidized at specified temperature in air.

The rate constant k_p of both tests is plotted in Fig. 6 as a function of the inverse of temperature ($1/T$). The activation energy of the oxidation in air and in pure oxygen is 195 ± 15 kJ/mol and 200 ± 10 kJ/mol, respectively. The activation energy values are nearly identical, but greater than that (130 kJ/mol) of LaB_6–ZrB_2 composites reported in literature.[8] The diffusion control mechanism of the LaB_6 oxidation takes place due to the presence of dense oxide scale (either glassy or crystalline). Rich oxygen atmosphere favors the formation of the oxidized layer. Without the layer or if the layer is in porous state, the oxidation is partially controlled by the

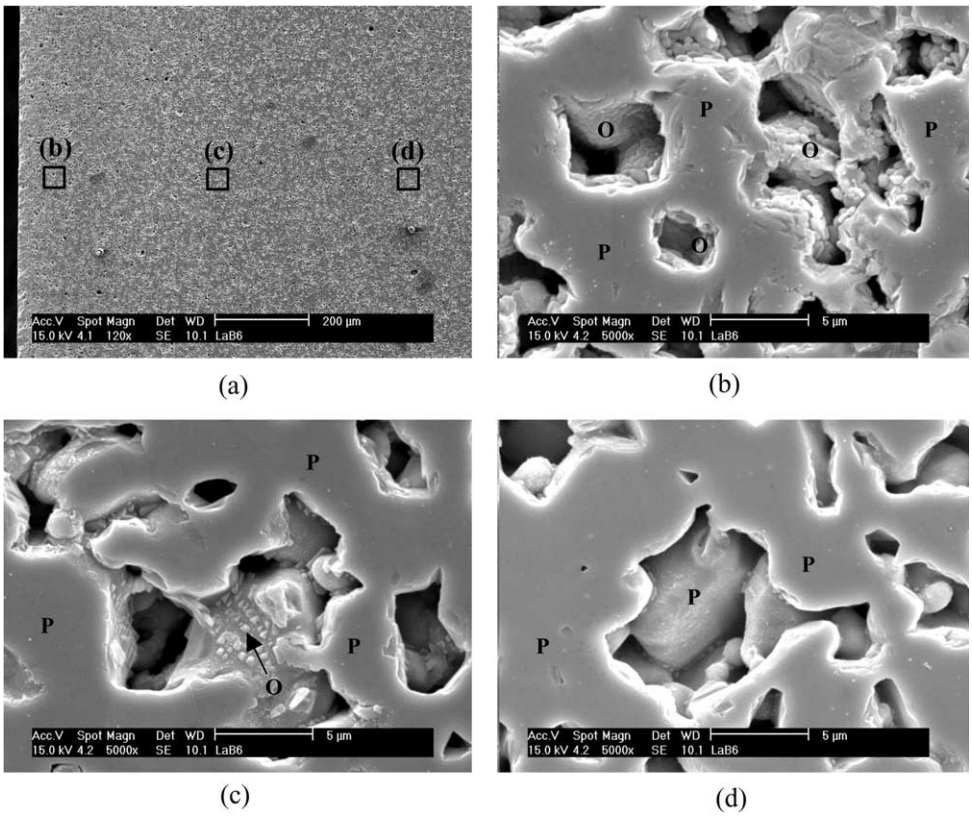

Fig. 8. SEM micrographs of the cross section of the sample calcined at 945 °C for 20 min in air with a flow rate of 100 mL/min. (b), (c), and (d) are the higher magnification images at different positions in (a) respectively. Where "P" represents the pure LaB_6, and "O" is oxide, La $(BO_2)_3$.

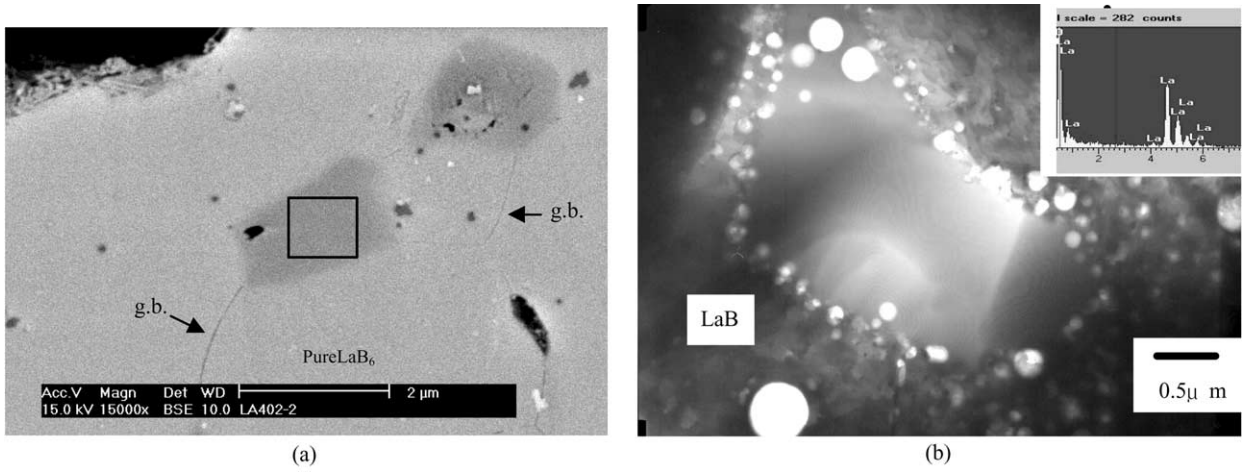

Fig. 9. (a) Back scattering SEM micrograph of the LaB_6 cross-section sample calcined at 800 °C for 40 min; (b) TEM BF micrograph of LaB_6 and EDS spectrum of the center glass pocket calcined at 800 °C for 4 min in airflow with air flow in 100 ml/min.

Table 3
Semi-quantitative EDS result of a glassy phase shown in Fig. 9(a)

Element	wt.%	at.%
B	38.16	79.80
O	8.10	11.45
La	53.74	8.75
Total	100.0	100.0

interfacial reactions. As a consequence, the time exponent of the reaction kinetics (Table 2) shows 1.25 to 1.7 in the other temperature regions.

3.2. Crystalline phase evolution

Fig. 7 shows the XRD results of oxidized LaB_6 from 800–1138 °C. The original pattern of LaB_6 is also shown at the bottom of Fig. 7, which is a cubic structure by the JCPD file.[9] When the testing temperature is higher than 700 °C, oxide layer starts to produce, as predicted by previous TGA tests. At the temperatures of $\geqslant$945 °C, a compound ($La(BO_2)_3$)[10] with monoclinic structure is formed, which is consistent with the report by Levin et al.[11] From the XRD results, the reaction in stoichiometry can be simply shown as below.

$$2LaB_6 + 10.5O_2 \rightarrow 2La(BO_2)_{3(crystal)} + 3B_2O_{3(glass)} \quad (3)$$

But later electron microscopic observation provides the composition of the newly-formed glass to be rich in La. It means that the first reaction product is La–B–O glass. The $La(BO_2)_3$ crystals nucleate and grow from the La–B–O glass afterward. The reaction can be expressed more precise as below.

$$2LaB_6 + 10.5O_2 \rightarrow La_2\text{–}B_{12}\text{–}O_{21(glass)} \rightarrow xLa(BO_2)_{3(crystal)} + La_{2-x}B_{12-3x}O_{21-6x(glass)} \quad (4)$$

The melting temperature of B_2O_3 is ca. 450 °C. B_2O_3-species may evaporate in the oxidation process when the temperature is higher than 1000 °C.[12] When the temperature is close to 1000 °C, the evaporation of B_2O_3 could be obvious.[13] Therefore, the oxidation mass change might be a result of the evaporation of B_2O_3 at the temperatures $\geqslant$995 °C. Then, part of the curves in Fig. 3(b) does not obey the parabolic law.

One cross section of partially oxidized LaB_6 is prepared and shown in Fig. 8(a). The bulky sample has been calcined at 945 °C for 20 min. The left side is the surface of the sample exposed to oxidation. The features of oxide scale revealed by the images appear less visible in the pores far away from the skin layer. Based on this evidence, it is concluded that the oxidation is only limited on the skin layer which is about 100 μm deep.

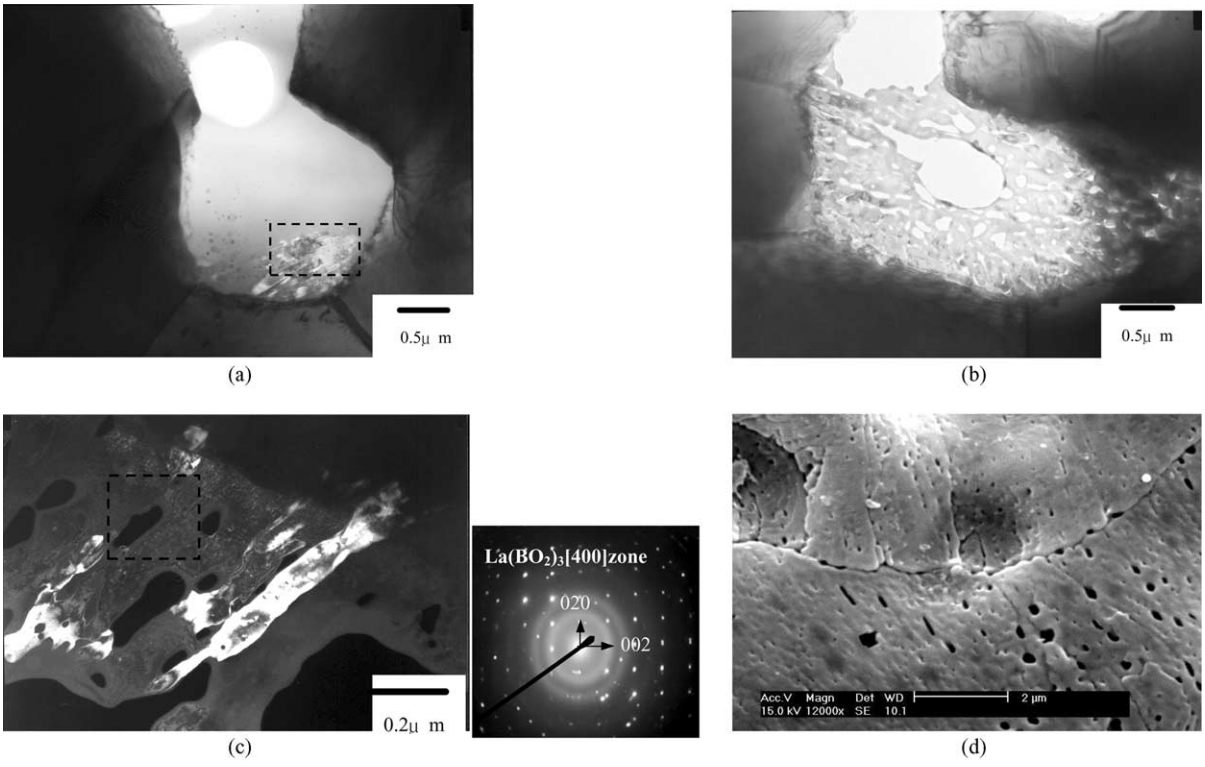

Fig. 10. TEM micrographs of LaB_6 calcined at 800 °C for 8 min in airflow. The BF images show (a) both oxide and glassy phase in the center, and (b) nearly crystallized region with micro-porosity. (c) The DF image of column shaped with a $La(BO_2)_3$ phase indexing as the diffraction pattern. (d) SEM micrograph of the oxide scale on the LaB_6 surface oxidized at 800 °C for 20 min.

3.3. Microstructure evolution of oxide scale

The TEM image [Fig. 1(b)] reveals the grains of LaB_6 in sizes about 3–5 μm. The diffraction pattern (DP) in Fig. 1(c) shows the 4-fold symmetry of the LaB_6 crystal. In addition to the micrometric open pores appeared in Fig. 1(b), there are some closed pores remained inside of the grains. Those submicron pores do not connect each other. They can be the residue from incomplete sintering.

There is an evidence of glass segregation, as shown in Fig. 9. The back scattering electron (BSE) micrograph of the polished cross-section surface [Fig. 9(a)] appears that the dark features at the center and upper right-hand-side of the image is the glassy phase. The composition of the region analyzed by EDS shows rich in O and La contents. It is believed that the position is originally a pore, which may fill in liquid phase (La–B–O glass) during oxidation. The light gray features are the grains of pure LaB_6. From the EDS result (Table 3), the glassy phase composed of La, B and O, and residual pores.

The detail observation of TEM microstructure is shown in Fig. 9 (b). There was a glassy region in the center of the BF image with size of 2–3 μm in diameter, which might be a hole originally. The glassy phase filled in the open holes, but remained small porosities from the evaporation of glassy phase. The neighboring LaB_6 grains were oxidized. The inserted EDS spectrum [Fig. 9 (a) (b)] shows the composition of the glassy phase at the center. The glassy phase composes of La, O, and possibly B. Because the element, boron, can not be detected by this EDS equipment, we still can infer that the glassy phase could include B content. Part of the reasons is that the melting temperature of pure La_2O_3 is 2305 °C,[14] which would not melt at 800 °C.

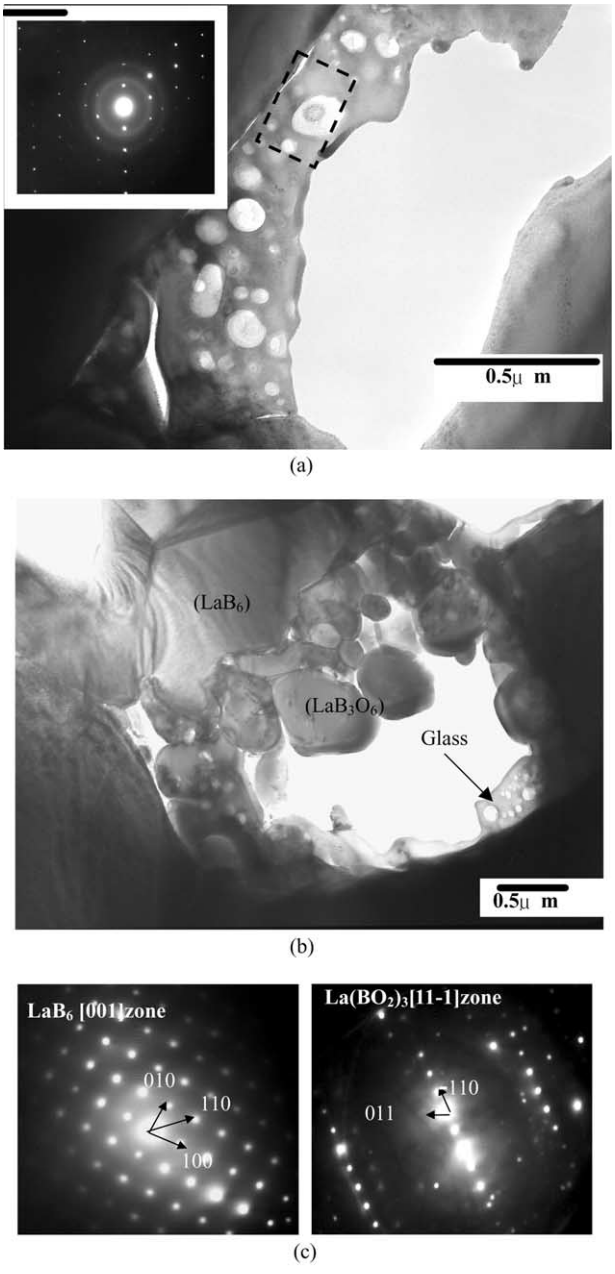

Fig. 11. TEM micrographs of LaB_6 calcined at 945 °C for (a) 30 s (b) 8 min in airflow. The inserted diffraction pattern shows the $La(BO_2)_3$ phase of the particle in the indicated region. (c) The correspondent DP of the regions shown in (b), either pure LaB_6 or oxide scale, $La(BO_2)_3$.

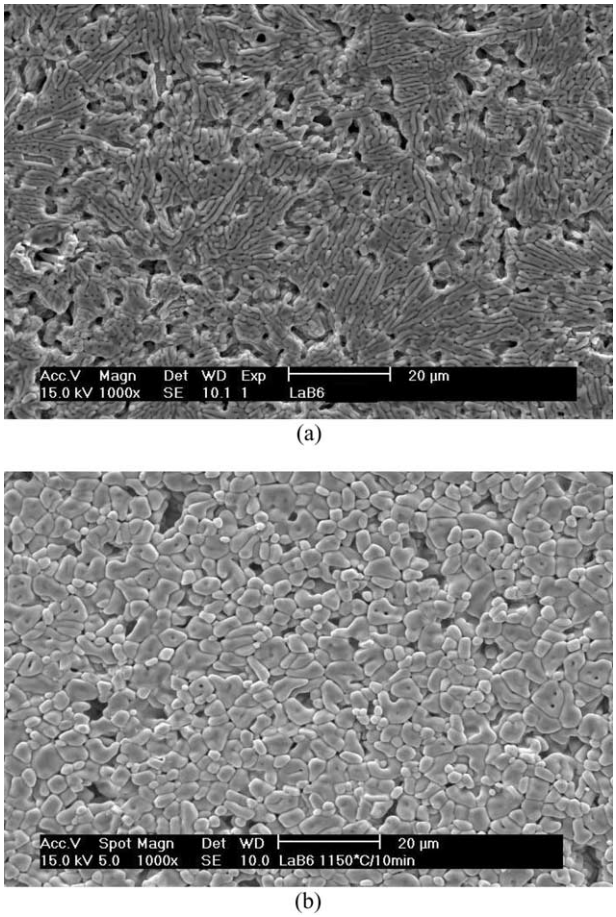

Fig. 12. SEM micrographs of LaB_6 samples calcined at 1138 °C for (a) 2 min or (b) 10 min in airflow of 100 ml/min.

As the thermal treatment takes longer time, the glass starts to crystallize. One example of the glass calcined at 800 °C for 8 min appears that the initial glassy phase fills the large pores and leaves a hole in the glass [Fig. 10(a)]. At the bottom of the glassy phase, there are some crystalline grains, of which show the $La(BO_2)_3$ phase proven by electron diffraction. It is also noted that the grains grow to columnar shape. The evidence provides that new oxide crystals are produced from the glassy phase when the heat treatment is longer than a few minutes.

Fig. 10(b) shows the other area of the same sample. The microstructure of the region indicates more oxidation. The glassy phase in the image almost changes to crystalline phase. The centered dark field (CDF) image from Fig. 10(c) of higher magnification shows the oxide grains with similar columnar shape, which implies those grains being in same orientation. The crystals nucleate from the glassy phase, lots of irregular small pores also produced at the same time. The small pores accompanies with the crystal phase is in the sizes of 0.1–0.2 μm. The features are clearly visible on the surface of 800 °C oxidized sample, as shown in Fig. 10(d). The fine porosity can be the results of density change of crystals to glass, or the evaporation of B_2O_3 volatile species.

As the oxidation conducted at 945 °C, the sample shows similar features, but different $La(BO_2)_3$ grain and more in porosity (Fig. 11). Thin and porous glass layer is produced on LaB_6 grain which have been oxidized for 30 s in air [Fig. 11(a)]. Small nano-grains grow from the amorphous phase, which is proven by the DP inserted in the figure. The glassy phase is not well adhered on the non-oxidized LaB_6 grain. It maybe due to the quick oxidation and/or mismatch of thermal expansion coefficient (CTE) between the glass (B_2O_3) and $La(BO_2)_3$.

Fig. 11(b) shows the TEM micrograph of the sample calcined at 945 °C for 8 min in airflow. Little liquid phase remains at the $LaB_6/La(BO_2)_3$ interface. This implies glass vaporizes apparently at this temperature Besides, the $La(BO_2)_3$ grains appear that the grain sizes are about $\leqslant 0.5$ μm and in equiaxial shape, which is different from the columnar grains produced at 800 °C. The grains grow to larger size at 945 °C

3.4. Oxidation microstructures near melting of $La(BO_2)_3$

$La(BO_2)_3$, which melts at 1141 °C, is the newly form crystalline phase in the oxide scale on LaB_6 surfaces. As tested at 1138 °C for 2 min, the SEM micrographs of the oxidized surface is shown in Fig. 12, which shows very few open pores remaining on the surface, and the pore sizes are smaller than those on pure LaB_6. The shape of the oxide products is vermicular in the appearance [Fig. 12(a)], which is similar to the features in Fig. 10. Besides, small submicron pores are observed, which may be caused by the evaporation of glassy phase, similar to the formation mechanism of pores in Fig. 10. When the sample treated at 1138 °C for longer period, e.g. 10 min [Fig. 12(b)], the surface produced different oxide grains which show dense and equiaxial features. The original open pores are sealed by the glass and new oxide products, which may undergo grain coarsening during the treatment.

When the sample is tested at 1185 °C, higher than the melting temperature (1141 °C) of $La(BO_2)_3$, the $La(BO_2)_3$ crystals start to melt. After rapid cooling, the morphologies are imaged by SEM and shown in Fig. 13. Glassy phase can be observed between grain boundaries. Almost all porosity is sealed. Only small bubbles are found on the surface [Fig. 13(b)] if prolong the treatment for 10 min. The melted phase can easily wet the grain boundaries and the bubbles maybe due to the evaporation of low-melting composition. During the oxidation process below 945 °C, the surface area would not change too much to affect the results. But as the oxidation takes place at the temperatures close to the melting of $La(BO_2)_3$, the oxidation nearly stop instantly due to the cover of dense $La(BO_2)_3$ crystals and glassy phase.

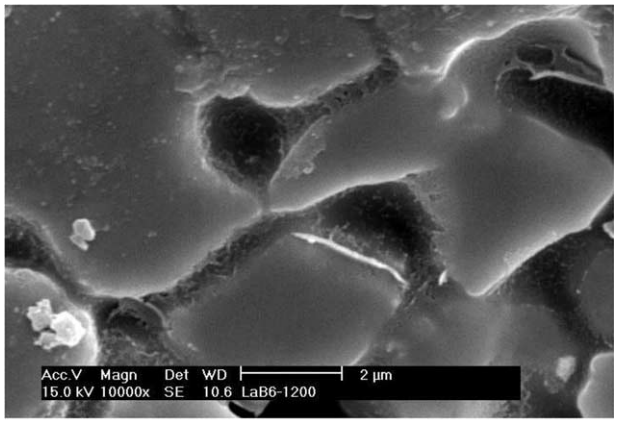

(a)

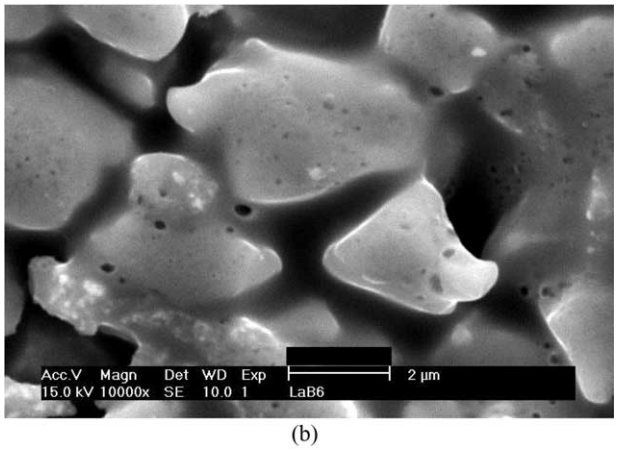

(b)

Fig. 13. SEM micrographs of LaB_6 samples tested at 1185 °C for (a) for a few seconds, or (b) 10 min in airflow of 100 mL/min.

4. Conclusion

From the results of TGA, TEM and SEM analysis, LaB_6 reacts with oxygen above 700 °C in air. The oxidation behavior obeys parabolic law in the range of 800–945 °C. The parabolic rate constant k_p, gives an oxidation activity energy $Q = 195 \pm 15$ kJ/mol in airflow and in pure oxygen atmosphere. Below 850 °C and higher than 995 °C, the oxidation behavior is partially influenced by the interfacial reactions, either the oxidation of surface LaB_6 or the evaporation of B_2O_3 glass. The oxidation mass gain gradually vanishes and the oxidation kinetic deviates away from the parabolic behavior as testing period prolongs.

The microstructural results reveal that as-received LaB_6 bulky sample shows 13 vol.% open porosity. Most of the pores are sealed as the testing close to the melting temperature (1141 °C) of $La(BO_2)_3$. La-B-oxide glass forms immediately, followed columnar $La(BO_2)_3$ grains grow in the glass. The boron glass apparently evaporates above 945 °C, gradually alternate the controlling mechanism of the oxidation to surface evaporation of the glass. Small and isolated porosity is formed in accompany with the grain coarsening of $La(BO_2)_3$ grains as the temperature is greater than 945 °C.

Acknowledgements

The authors are grateful to thank the use of TGA offered by CSIST and the funding supported by National Science Council in Taiwan under the contract NSC92-2216-E-002-026

References

1. Campbell, I. E., Sherwood, E. M. In *High-Temperature Materials and Technology*, Part III, 10. John Wiley and Sons, Inc., New York, London and Sydney, pp. 349–359.
2. Berkowitz-Mattuck, J. B., High-temperature oxidation III. *zirconium and hafnium diborides. J. Electrochem. Soc.*, 1966, **113**(9), 908–914.
3. Kuriakose, A. K. and Margrave, J. L., The oxidation kinetics of zirconium diboride and zirconium carbide at high temperatures. *J. Electrochem. Soc.*, 1964, **111**(7), 827–831.
4. Tripp, W. C. and Graham, H. C., Thermogravimetric study of the oxidation of ZrB_2 in the temperature range of 800 °C to 1500 °C. *J. Electrochem. Soc.*, 1971, **118**(7), 1195–1199.
5. Kulpa, A. and Troczynski, T., Oxidation of TiB_2 powders below 900 °C. *J. Am. Ceram. Soc.*, 1996, **79**(2), 518–520.
6. Tampieri, A. and Bellosi, A., Oxidation of monolithic TiB_2 and of Al_2O_3-TiB_2 composites. *J. Mater. Sci.*, 1993, **28**, 649–653.
7. Tampieri, A., Landi, E. and Bellosi, A., On the oxidation behavior of monolithic TiB_2 and Al_2O_3-TiB_2 and Si_3N_4-TiB_2 composites. *J. Therm. Anal.*, 1992, **38**, 2657–2668.
8. Chen, C. M., Zhang, L. T., Zhou, W. C., Li, M. Q., Hao, Z. Z., Jiang, Y. J. and Yang, S. L., Microstructure performance and oxidation mechanism of boride in situ composites. *Composites Science and Technology*, 2001, **61**, 971–975.
9. Philips Export B. V., JCPD file of LaB_6, 34-0427, 1990.
10. Philips Export B. V., JCPD file of La $(BO_2)_3$, 23-1140, 1990.
11. Levin, E. M., Robbins, C. R. and Waring, J. L., Immiscibility and the system lanthanum oxide-boric oxide. *J. Am. Ceram. Soc.*, 1961, **44**(2), 89.
12. Chen, C.-M., Zhang, L. T., Zhou, W. C. and Li, M. Q., High temperature oxidation of lab_6-zrb_2 eutectic in situ composite. *Acta Mater.*, 1999, **47**(6), 1945–1952.
13. Soulen, J. R., Sthapitanonda, P. and Margrave, J. L., *J. Am. Chem. Soc.*, 1995, **59**, 132–136.
14. Campbell, I. E., Sherwood, E. M. In *High-Temperature Materials and Technology*, Part III, 10. John Wiley and Sons, INC., New York, pp. 349–359.